JETIR.ORG ISSN: 2349-5162 | ESTD Year : 2014 | Monthly Issue
JOURNAL OF EMERGING TECHNOLOGIES AND INNOVATIVE RESEARCH (JETIR)
An International Scholarly Open Access, Peer-reviewed, Refereed Journal

Synthesis, Characterization and Anticorrosion Studies of Furfuryl Based Methacrylate Copolymer and its Titania Nanocomposites

[1]G.D. Babu, [2]B. Ranjith Kumar, [1]P. Mohamed Ashfaque, [1]K. Mohammed Rehan, [1]K. Abdul Wasi, [1]S. Mohammed Safiullah, [1]K. Anver Basha*

[1] P.G. and Research Department of Chemistry, C. Abdul Hakeem College (Autonomous), Affiliated to Thiruvalluvar University, Vellore, India.

[2]Department of Chemistry, Chennai Institute of Technology (Autonomous), Kundrathur, Chennai.

Abstract : Methacrylate based polymer nanocomposite coatings have emerged as a prominent material in corrosion science in recent years. In this article, an attempt has been made to study the anti-corrosive properties of poly(furfuryl methacrylate-co-glycidyl methacrylate)/TiO_2 nanocomposite (poly(FMA-co-GMA)/TiO_2) prepared by in-situ solution polymerization method. To which the oleic acid (OA) modified titanium oxide nanoparticles (OA-TiO_2) were incorporated during the solution polymerization with different ratios using chlorobenzene as solvent, and AIBN as initiator. The Nuclear magnetic resonance spectroscopy (^{1}H and ^{13}C NMR), Fourier Transform Infrared Spectroscopy (FTIR) and X-ray diffraction (XRD) studies confirmed the formation of poly(FMA-co-GMA) and its TiO_2 composites. The electrochemical characteristics of poly(FMA-co-GMA)/TiO_2 composites film coated on mild steel specimens were investigated and compared with poly(FMA-co-GMA) coated substrate in 3.5% NaCl solution using Tafel and electrochemical impedance spectroscopic (EIS). The morphology of the nanocomposites was confirmed by Scanning electron microscopy (SEM) and Energy dispersive X-ray based elemental mapping. The EIS studies shows that the modified TiO_2 nanoparticles, poly(FMA-co-GMA)/TiO_2 coated on mild steel provides tremendous protection against corrosion in 3.5% NaCl than the copolymer coated (or) bare specimens.

Keywords **-** Furfuryl methacrylate, Glycidyl methacrylate, Impedance spectroscopy, Tafel plot, Nyquist plot.

INTRODUCTION

The metallurgical and electrical industries have shown much interest in the topic of corrosion control. Metal corrosion is a pressing problem as it has a significant economic and environmental impact globally. Various forms of corrosion including wet corrosion, crevice corrosion, pitting corrosion, pipeline corrosion, and microbial assisted corrosion were merely associated with maritime environment [1]. To overcome this issue barrier protection characteristic are the prime tool which acts as a layer of protection between the metal and its surroundings. This limits ions from the environment, including water, oxygen, and other ions, get into the metal surface. A prominent area of research in materials science is the development of hybrid materials to enhance coating stability and anticorrosive properties [2].

The most popular technique for providing improved protection for metals from corrosive environments is polymer coating [3]. Developing a high-end engineering polymeric material that is eco-friendly, biosafe, and non-toxic are of utmost importance as protective coatings in corrosion research due to more onerous environmental requirements [4]. This layer serves as a barrier between the metallic surface and corrosive ions in a stringent environment against corrosion. The polymer-based coatings are chromate-free, have great chemical resistance, and have strong adhesion to a variety of metallic substrates makes them suitable options [5].

Methacrylate copolymer coatings are a form of protective coating that improves the corrosion resistance of mild steel, lowers maintenance costs, and offers long-lasting defense against corrosion. Furfuryl methacrylate (FMA) is an important monomer in polymer chemistry and has been studied extensively due to its unique properties and potential applications in numerous fields [6,7]. FMA has an excellent thermal stability and high glass transition temperature, making it suitable for use in high-temperature applications such as adhesives, coatings, and composites.

By reducing porosity and weaving the diffusion channel for corrosive species like oxygen and chloride anions, the incorporation of nanoparticles in polymeric coatings can significantly increase their barrier performance [8, 9]. Composite coatings add a lot of micro-fillers to the polymer matrix in order to attain the desired anti-corrosion qualities [10].

It is obvious that highly dispersed nanocomposites show exceptional anticorrosive behavior, which reflects in this study. The prime theme of this article is to assess the anticorrosive performance of poly(FMA-co-GMA)/TiO_2 composite film coated on mild steel specimens and compared with poly(FMA-co-GMA) coated substrate in 3.5% NaCl solution using Tafel and electrochemical impedance spectroscopic (EIS) studies.

EXPERIMENTAL

Materials

Furfuryl methacrylate purchased from Sigma Aldrich was purified by high vacuum distillation, Glycidyl methacrylate was distilled under vacuum and 2,2'-azobis(isobutyronitrile) (AIBN) (Sigma Aldrich) was purified and recrystallized from ethanol. Chlorobenzene obtained from BDH laboratories, which was used without further purification. The anticorrosive property of the copolymer and its nanocomposites coated on mild steel (MS) in 3.5% (W/V) in NaCl were carried out.

Synthesis of the Furfuryl methacrylate (FMA)

The synthesis of the Furfuryl methacrylate from furfuryl alcohol and methacryloyl chloride is as follow. The synthesized furfuryl methacrylate is insoluble in water and soluble in most of the organic solvents. The monomer is characterized by FT-IR, ^{1}H-NMR and ^{13}C-NMR The structure of the compound is given in **Scheme. 1**.

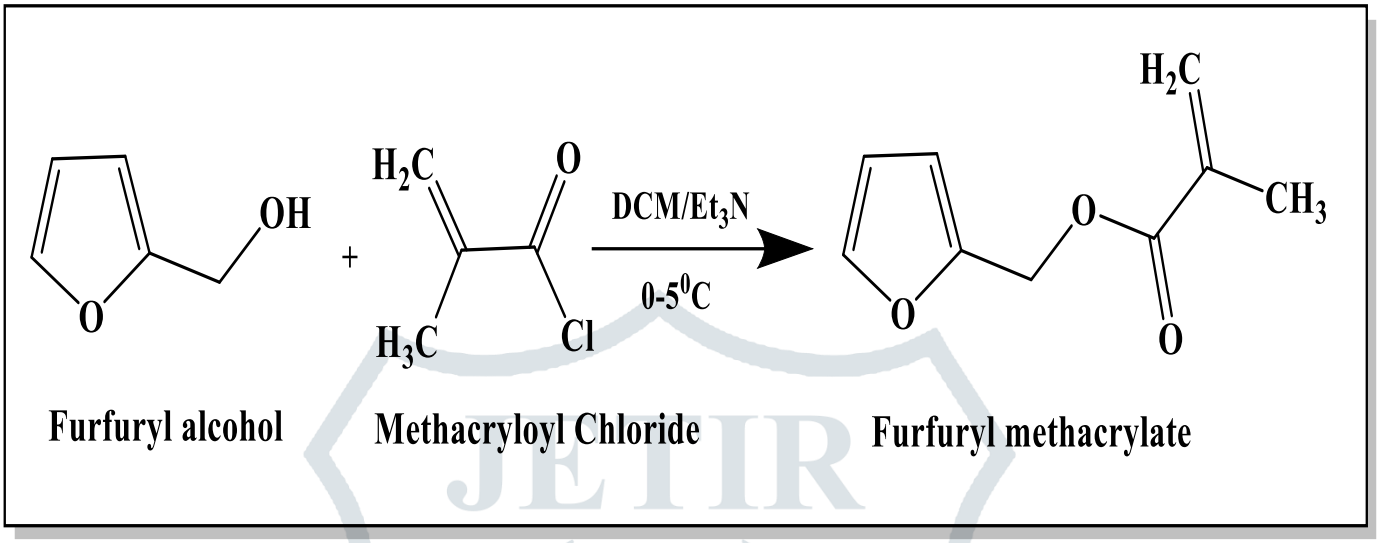

Scheme. 1: Synthesis of the Furfuryl methacrylate (FMA)

^{1}H NMR (300 MHz, $CDCl_3$) d ¼ 7.4 (s, 1H, —CH–O– of furan ring), 6.3 (m, 2H, —CH–CH— of furan ring), 4.9 (s, 2H, O–CH_2– of PFMA), 3.5 (s, 3H, O–CH_3 of PMMA), 0.9–1.9 (different aliphatic protons of the methacrylate unit).

^{13}C NMR (300 MHz, $CDCl_3$) d ¼ 177.65 (>CO), 149.33 (–C- of furan ring), 110.33 (>CH– of furan ring), 143.60 (>CH– of furan ring), 125.90 (O–CH_2 of PFMA unit), 52.12 (O–CH_3 of PMMA unit), 58.68 (–CH_2– of the methacrylate unit), 45.15 (>C< of the methacrylate unit), 18.91 and 17.85 (atactic structure of a-CH_3 side chain).

FT-IR (KBr): 3 122, 2 957, 1 727, 1 501, 1 153, 1 012, 919, 816, 746 cm^{-1}.

Surface modification of Titanium oxide nanoparticles

Surface modification of TiO_2 nanoparticle were carried out with oleic acid [11]. 50ml of 2% solution of oleic acid was prepared in ethanol. To this solution 0.5g of Titanium oxide nanoparticles (TiO_2 NPs) was added and stirred at 50^{0}C. After 4 h the contents were centrifuges (1 x 10^{6}rpm) the grafted TiO_2 nanoparticle were collected and washed with ethanol followed by acetone (5 x 30ml) and dried under reduced pressure (**Scheme. 2)**.

Synthesis of Poly (FMA-co-GMA):

The copolymer was synthesized by free radical solution polymerization [12, 13]. The required amount of monomers Furfuryl methacrylate and Glycidyl methacrylate were dissolved in chlorobenzene along with the initiator AIBN in a polymer tube as shown in **Scheme 3.**

Synthesis of Furfuryl methacrylate nanocomposite:

Poly(FMA-co-GMA)/OA-TiO_2 were prepared (**Scheme. 4)** by the addition of different moles of Furfuryl methacrylate, Glycidyl methacrylate (0.20:0.80, 0.50:0.50, 0.80:0.20) and 5 wt.% of OA-TiO_2 in 50ml chlorobenzene solvent. Further the solution was kept for ultra-sonication for 30 min, then polymerization was carried out at 60^{o}C using AIBN as radical initiator under N_2 atmosphere (2hr). After cooling, white coloured amorphous powder was obtained by the addition of hexane, it was further re-precipitated from chloroform to get the pure product.

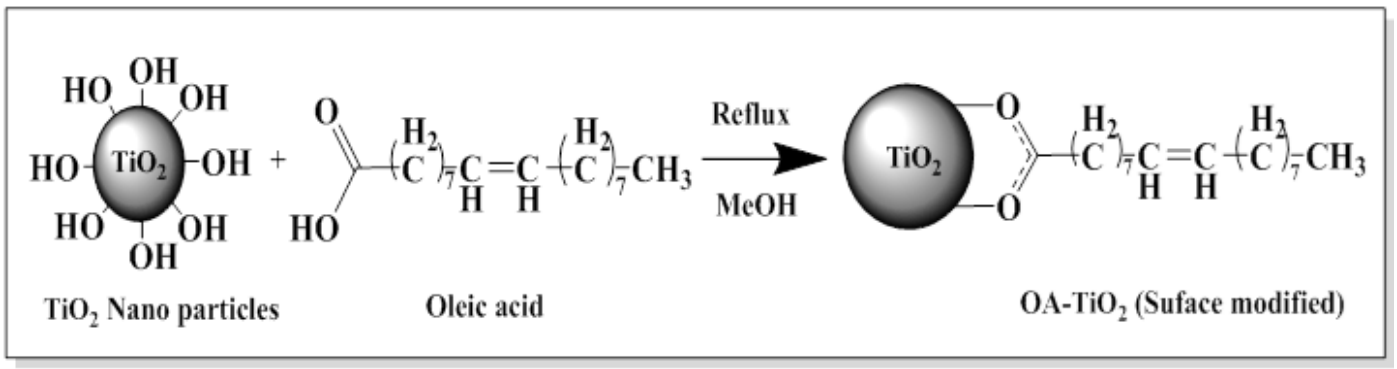

Scheme. 2: Surface Modification of TiO_2

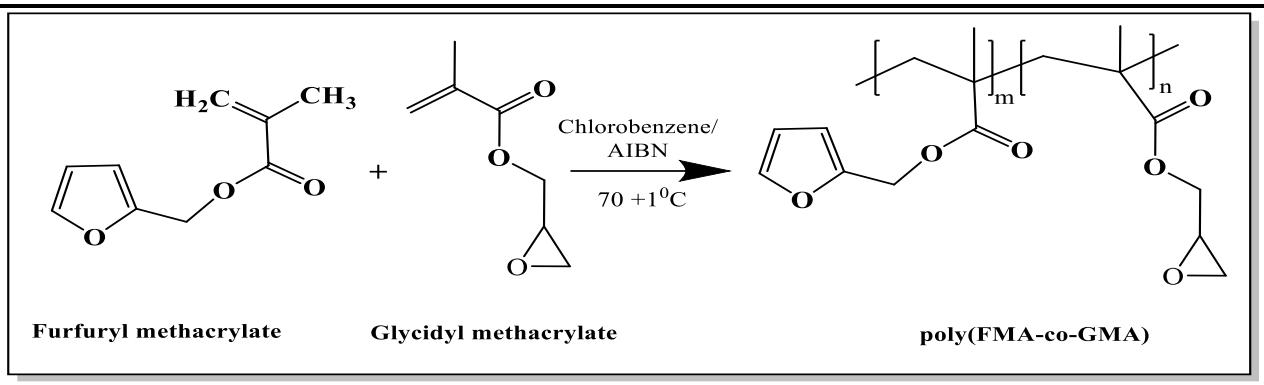

Scheme. 3: Synthesis of the poly(FMA-co-GMA)

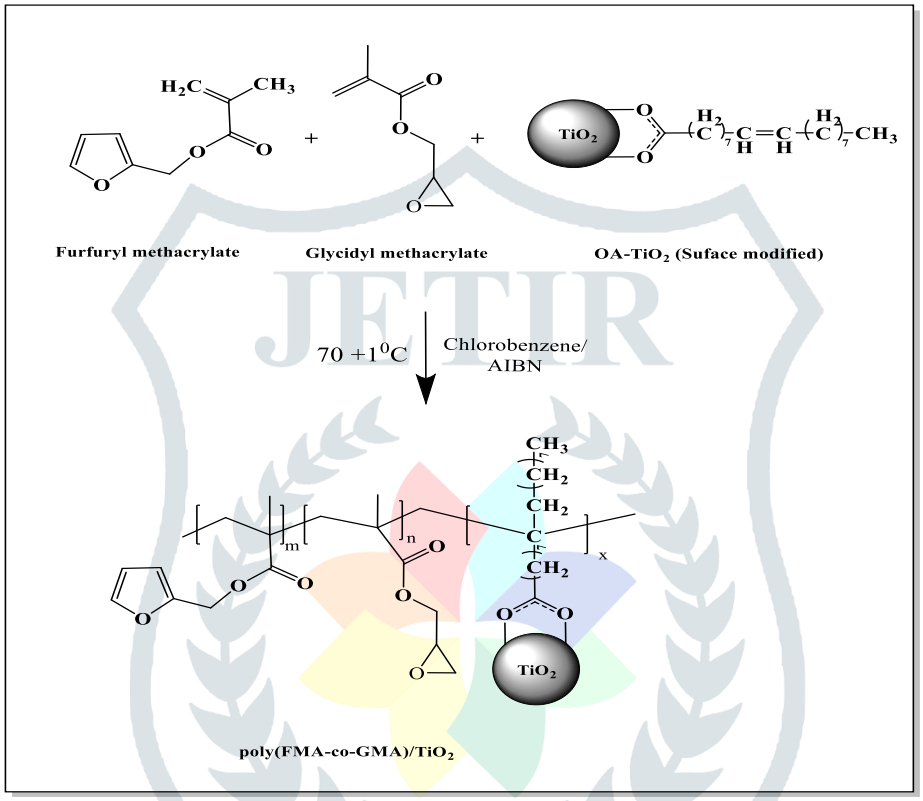

Scheme. 4: Synthesis of the poly(FMA-co-GMA)/TiO_2 Nanocomposite

RESULT AND DISCUSSION:

^{1}H NMR Spectroscopy:

Synthesized poly(FMA-co-GMA) were characterized by ^{1}H NMR spectra taken on a Bruker-Instrument-NMR Spectrometer (DPX400) with DMSO as the solvent. In **Fig 1:**

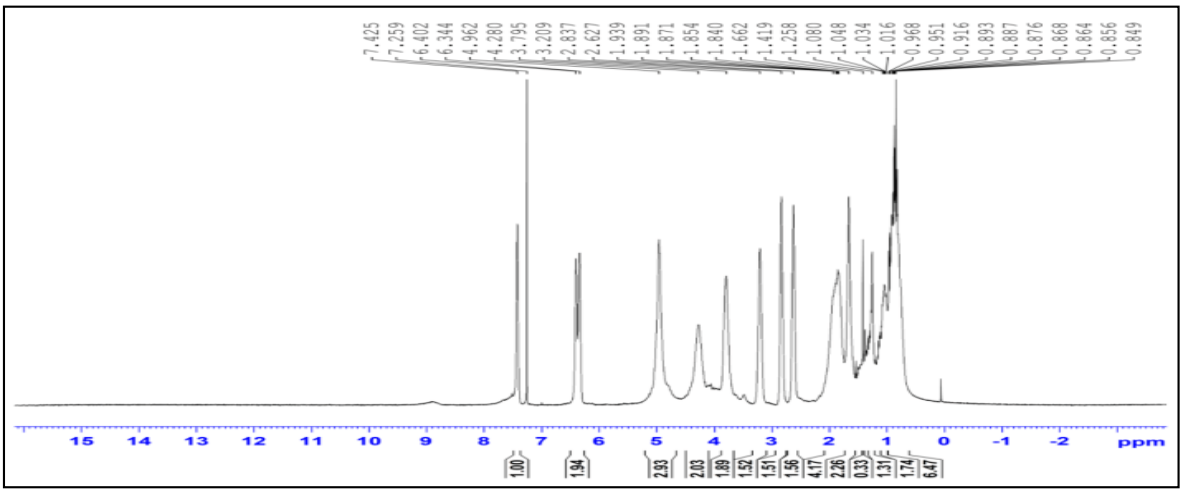

Fig. 1: ^{1}H-NMR Spectrum of the poly(FMA-co-GMA)

^{1}H NMR (300 MHz, CDCl3) d ¼ 7.4 (s, 1H, —CH–O– of furan ring), 6.3 (m, 2H, —CH–CH— of furan ring), 4.9 (s, 2H, O–CH_2– of PFMA), 3.5 (s, 3H, O–CH_3 of PMMA), 0.8–1.9 (different aliphatic protons of the methacrylate unit).

^{1}H NMR spectrum of poly(FMA-co-GMA) confirms the presence of pyrrole ring (m, 4H), The peaks at 0.7 to 1.9 ppm are due to the different saturated protons (–CH_3 and –CH_2–) of the methacrylate units of poly(FMA-co-GMA). The peaks at 7.4 and 6.3 ppm correspond to the different aromatic protons of furan ring. The spectrum shows two signals at 4.28 and 3.79 ppm, which are due to –$COOCH_2$ – group at GMA units [14]. The peak at 3.209 ppm is due to the methylene proton of the epoxy group. The methylene protons of the epoxy group show signals at 2.72 and 2.60 ppm. The backbone methylene groups show signals at 1.54 – 2.51 ppm. All of the copolymers were soluble in many of the organic solvents, such as THF, $CHCl_3$ and Toluene.

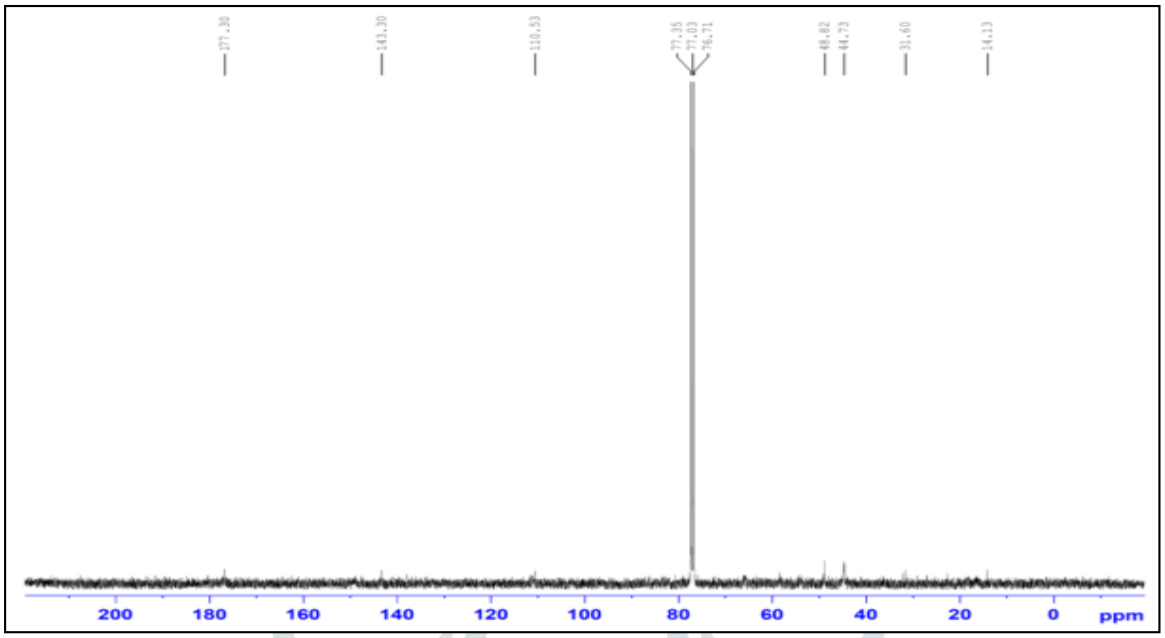

Fig. 2: ^{13}C-NMR Spectrum of the poly(FMA-co-GMA)

^{13}C NMR (300 MHz, $CDCl_3$) d ¼ 177.30 (>CO), 110.53 (>CH– of furan ring), 143.30 (>CH– of furan ring), 125.90 (O–CH_2 of PFMA unit), 44.73 (>C< of the methacrylate unit), 18.91 and 17.85 (atactic structure of a-CH_3 side chain).

The ^{13}C NMR spectrum of the poly(FMA-co-GMA) is shown in Figure 2. The ester carbonyl of GMA appeared at 177.7 ppm. The aromatic carbons of FMA unit in copolymer appeared at 143.3, 110.53, respectively. The methylene group of the epoxy group in GMA unit shows signal at 66.3 ppm.

FT-IR Spectroscopy:

A transmission vibrational spectrum of OA-TiO_2, poly(FMA-co-GMA), and poly(FMA-co-GMA)/TiO_2 are shown in Fig. 3.

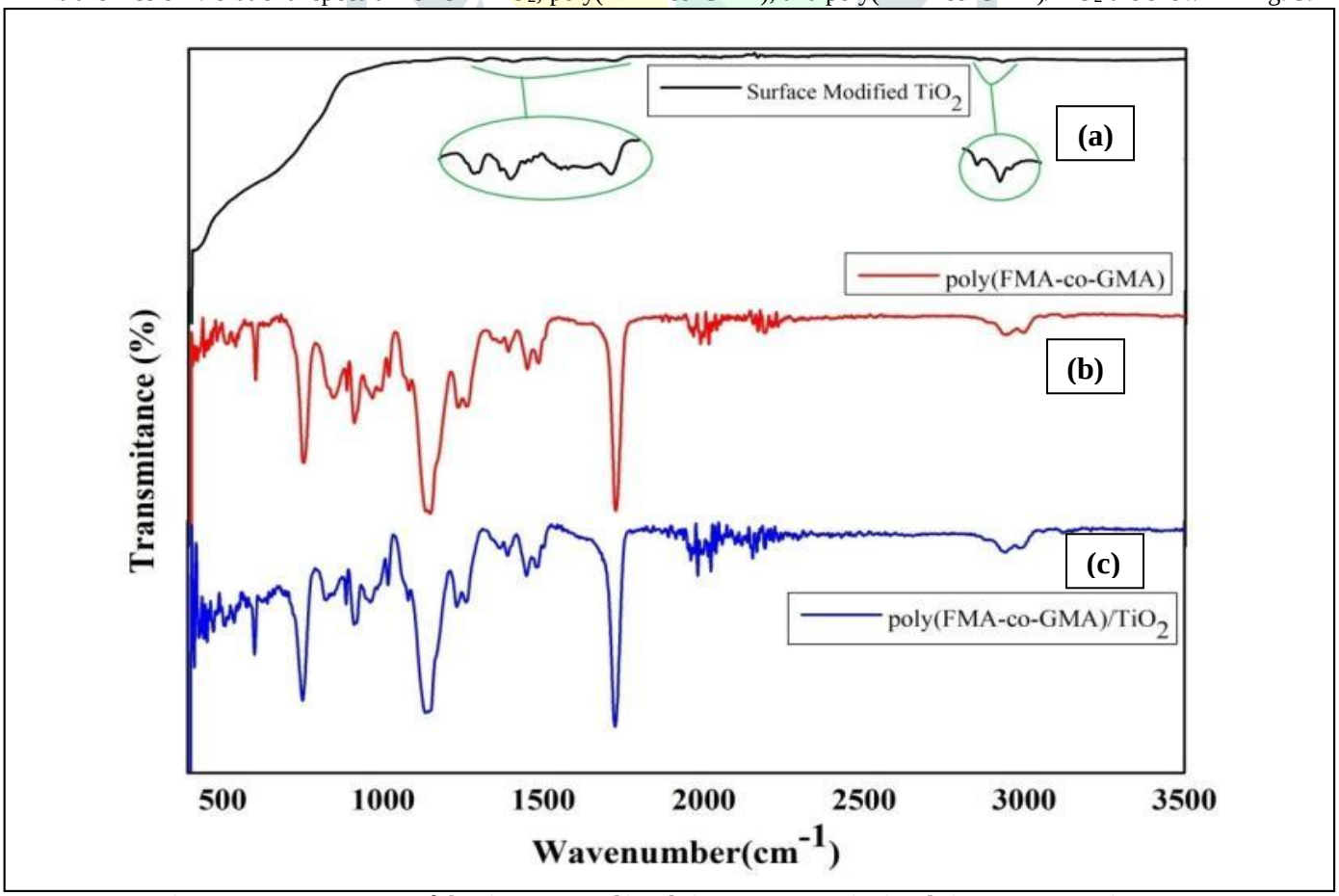

Fig. 3: FT-IR Spectrum of the a) OA-TiO_2, b) poly(FMA-co-GMA), c) poly(FMA-co-GMA)/TiO_2

FTIR analysis was employed to study the characterization of OA-TiO_2 nanoparticles, is shown in Figure 3a. The first band is the broadest, and is observed at 3500 cm^{-1}, corresponding to the stretching vibration of the hydroxyl group O-H of the TiO_2 NPs. The second band is observed around 1630 cm^{-1}, corresponding to bending modes of water Ti-OH and Ti-O bending mode vibration observed at 483cm^{-1}; the last is a prominent peak at 1398 cm^{-1} related to Ti-O modes [15]. The long alkyl groups in oleic acid were characterized in the peaks of 2929 cm^{-1} and 2857 cm^{-1}. Moreover, the adsorption peaks in 1713 cm^{-1} attributed to carbonyl groups of oleic acid in OA-TiO_2 nanoparticles [15] and –C=C- peak appeared at 1610cm^{-1}.

In Fig 3b. Shows FTIR Spectrum of poly(FMA-co-GMA). The vibration bands observed at 2996, 2937, and 1258 cm^{-1} are for the $–CH_3$ asymmetric and symmetric stretching and symmetric bending vibrations of methacrylate units, respectively. The vibration peak at 908 cm^{-1} is assigned to –CH bending vibrations, and the peak at 556 cm^{-1} is assumed to be related to the CH_3 (C–O) group. The C–H wagging vibration modes are confirmed by the presence of a band at 750 cm^{-1} [16]. Carbonyl groups gave strong peaks at 1723, 1144, and 1258 cm^{-1}, attributed to the stretching of the glycidyl methacrylate ester group. In Fig 3c, shows respective peaks of polymer nanocomposites confirms the FTIR Spectrum of poly(FMA-co-GMA)/TiO_2.

XRD Studies

XRD pattern of the crystalline structure of OA-TiO_2 nanoparticle, poly(FMA-co-GMA) and poly(FMA-co-GMA)/TiO_2 nanocomposites were shown in fig 4. the OA-TiO_2 exhibits the prominent peaks at around 24.61, 27.61, 36.26, 41.41, 54.56, 56.86 and 69.21 θ [11]. The average grain sizes (D) were determined by the Debye-Scherrer's equation.

$$Dc = 0.9\lambda/\beta\cos\theta$$

Where λ is the X-ray wavelength and is the β width of diffraction peak at its half maximum intensity.

In Figure 4b, the coexistence of a broad amorphous peak from poly(FMA-co-GMA) and suppressed crystalline peaks from TiO_2 confirms the excellent distribution and compatibility of TiO_2 within the resulting nanocomposite. The diffractogram of OA-TiO_2 nanoparticles and poly(FMA-co-GMA)/TiO_2 composites shows characteristic peaks of the anatase phase (major peaks: 25.4°, 38.0°, 48.0°, and 54.7°) and the rutile phase (2θ at 27.4°, 36.1°, 41.3°, and 54.4°) which demonstrating that the incorporation of TiO_2 nanoparticles in the poly(FMA-co-GMA)/TiO_2 composites is mixed types of anatase/rutile TiO_2 composites. The size of the crystals was 17nm based on estimation using Scherrer equation.

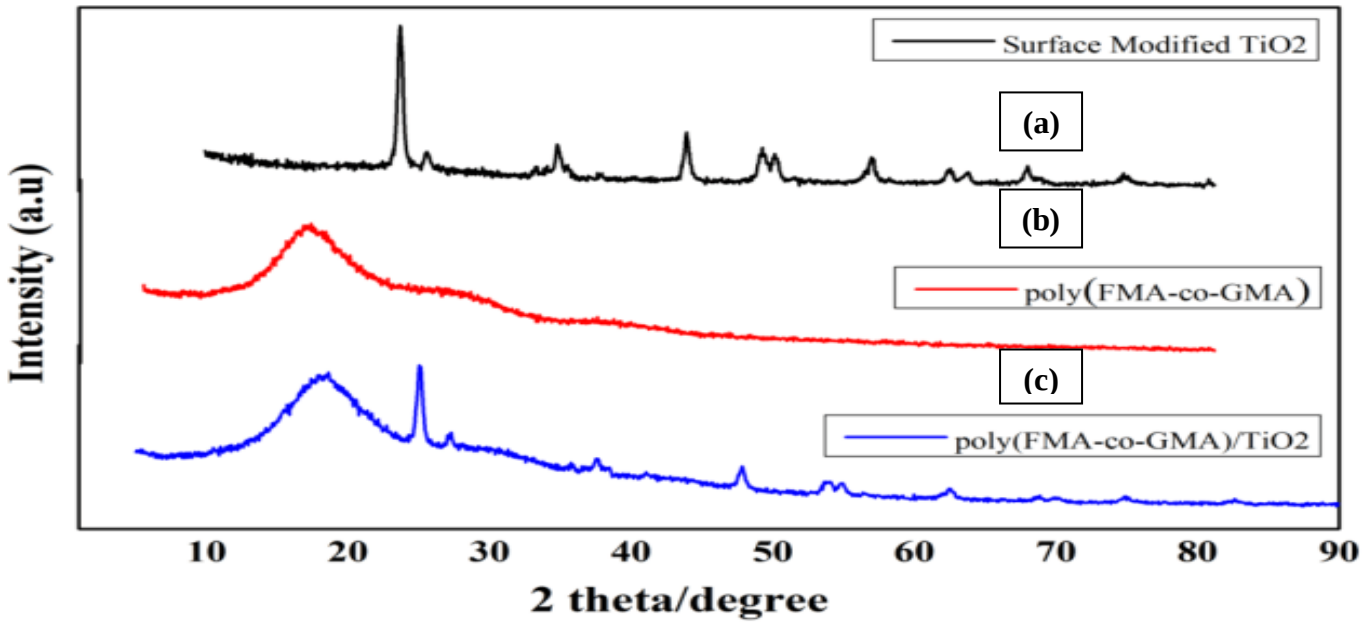

Fig. 4: XRD Spectrum of the a) OA-TiO_2, b) poly(FMA-co-GMA), c) poly(FMA-co-GMA)/TiO_2

Thermal Studies:

The thermal stability of the different copolymers and its nanocomposites were investigated by TGA. Figure 5 shows the TGA curves of poly(FMA-co-GMA) and poly(FMA-co-GMA)/TiO_2 the obtained results were summarized in Table 1. The TGA curve clearly shows that all the thermograms followed the three or four stage decomposition patterns.

It can be seen that the increase of FMA content increases the initial decomposition temperature, also increases the residual amount of char left out. The ratios of 20:80, 0.50:0.50 (FMA/GMA) copolymers showed initial weight loss, 3.89%, 3.75% at 101.5˚C, 105.3˚C respectively due to evaporation of water or solvent. The second stage decomposition starts from 302˚C to 320˚C, it's due to cleavage of furfuryl pentane groups, and the third stage decompositions start from 388 to 430˚C due to cleavage of polymer backbone chain.

Table 1. TGA Data of Copolymer (FMA-co-GMA) and its nanocomposites.

Obviously, it is observed that the thermal decomposition temperatures of polymer (0.80:0.20 (FMA/GMA)) are higher than that of poly(FMA-co-GMA)/TiO_2 composite material or else simply thermal stability of the copolymer increases as increases of furfuryl moieties in the copolymers.

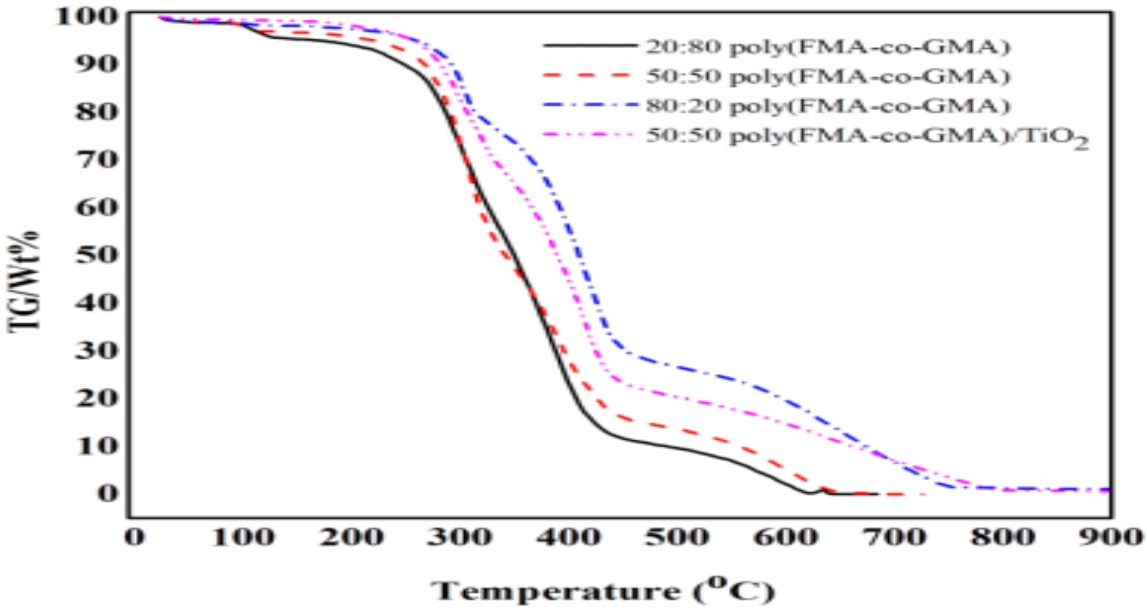

S.No.	poly(FMA-co-GMA)	*Tg* (°C)	IDT (°C)	Temperature (°C) at weight loss (%)				
				10%	30%	50%	70%	90%
1.	poly(FMA-co-GMA)-20:80	329	169	244	304	349	389	489
2.	poly(FMA-co-GMA)-50:50	327	175	265	305	340	394	555
3.	poly(FMA-co-GMA)-80:20	322	183	293	363	408	448	673
4.	poly(FMA-co-GMA)-50:50/TiO_2	306	182	282	332	387	424	657

Fig. 5: TGA Spectrum of the a) OA-TiO_2, b) poly(FMA-co-GMA), c) poly(FMA-co-GMA)/TiO_2

Fourier Emission- Scanning Electron Microscope (FE-SEM):

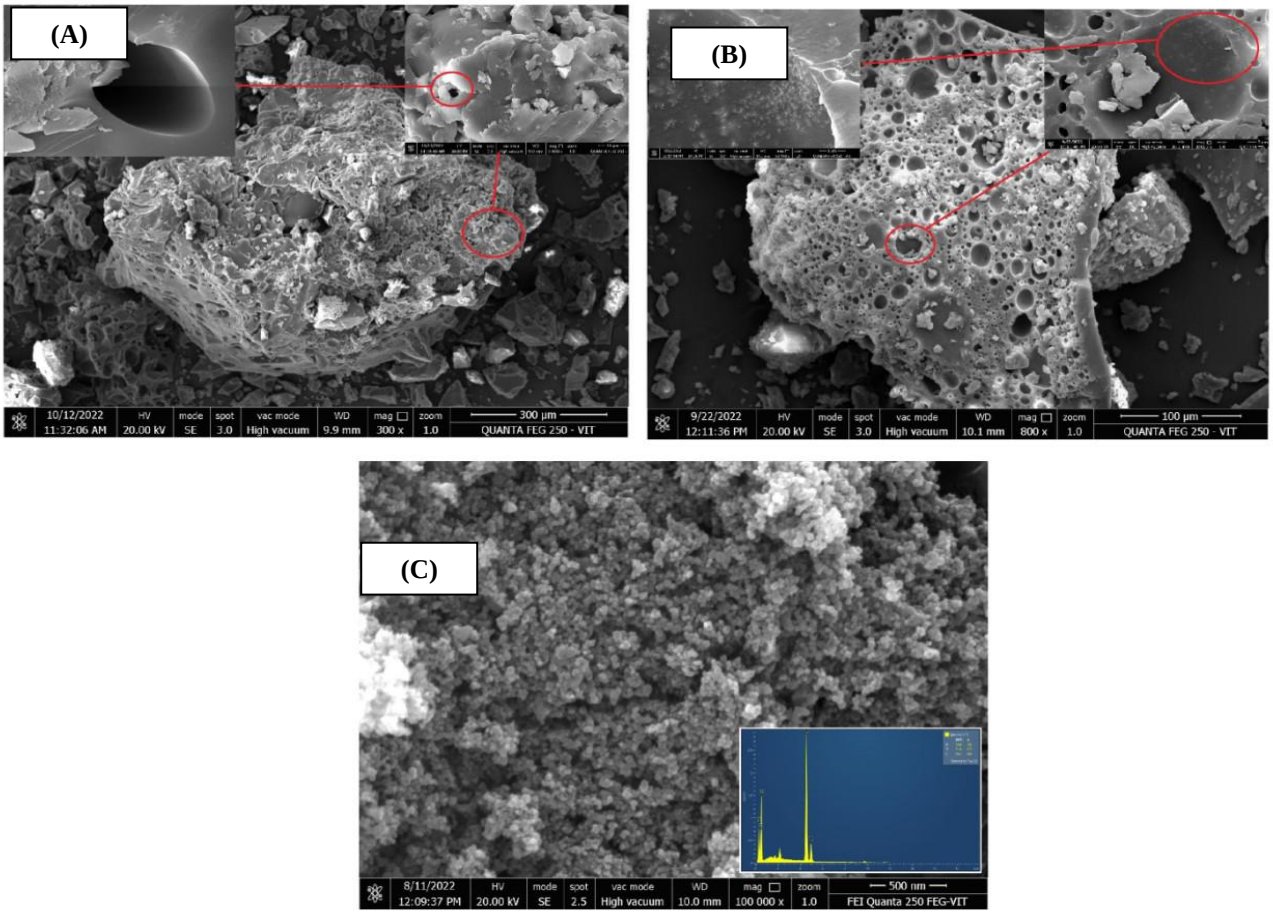

Fig. 6: SEM Images of solid a) poly(FMA-co-GMA), b) poly(FMA-co-GMA)/TiO_2, c) OA-TiO_2,

FE-SEM indicates that the surface of poly(FMA-co-GMA) exhibits a smooth and homogeneous texture (Fig 6a), while the poly(FMA-co-GMA)/TiO_2 (Fig 6b) composites display a highly rough and heterogeneous surface, indicating the successful incorporation of surface-modified nanoparticles.

The observed significant morphological changes in the composites can be attributed to the strong influence of the hydrophobic nature of TiO_2 nanoparticles added to the Poly(FMA-co-GMA) system, which enhances the compatibility between the polymer and OA-TiO_2 and impacts the overall composite morphology [11]. When examining the SEM image, the nanoparticles are evenly incorporated through entire surface of polymer composites can be visually observed at high magnification.

The FESEM images and EDX analysis of the surfaced modified OA-TiO_2 NPs show in Figure 6c. which confirms that the OA-TiO_2 NPs are spherical and highly uniform in size. In addition, the EDX analysis confirms, the peak of C shows the existence of OA functionality on the surface of TiO_2 NPs. Furthermore, the EDX analysis indicates that titanium (Ti), oxygen (O), and carbon (C) are the major constituents of the nanoparticles. which is also confirmed by FTIR.

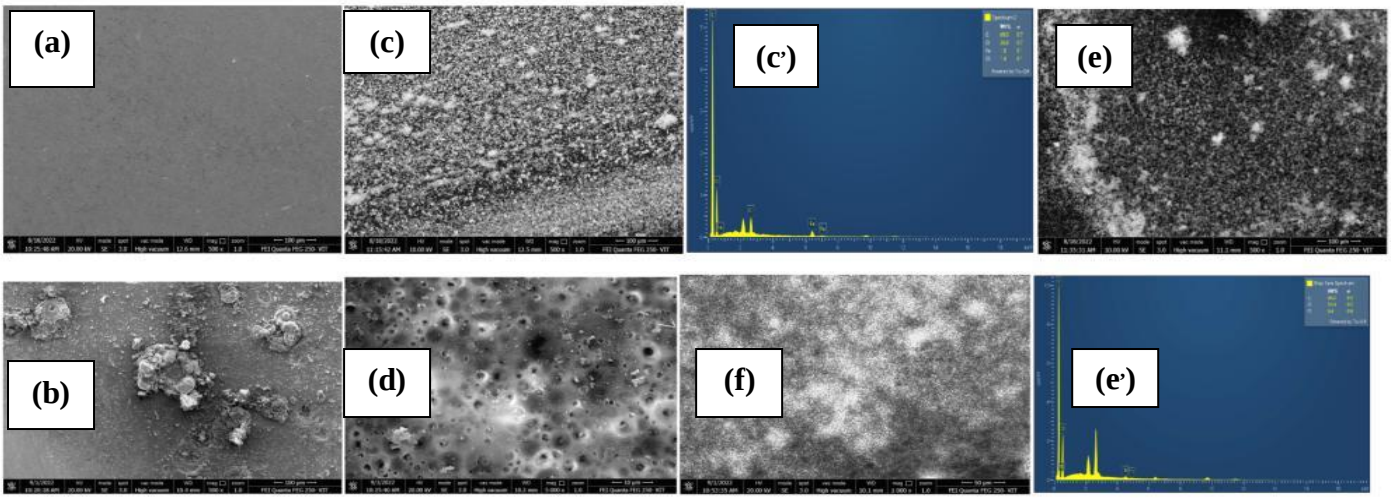

Fig. 7: SEM images of mild steel samples: (a) polishing surface (b) after corrosion studies in 3.5% NaCl solution, (c, d, e) polymer coated Mild steel before & after corrosion studies and its EDAX, (f) polymer coated Mild steel before corrosion studies

Surface morphology of bare and coated mild steel were studied by scanning electron microscopy before and after the corrosion studies in 3.5% NaCl. [17] Figure 7(a) displays the SEM image of the polished Mild steel sample prior to exposure to the corrosive environment. The image reveals a smooth surface with some abrasion scratches present. In contrast, Figure 3(b) exhibits significant damage on the surface of the mild steel sample resulting from the formation of corrosion products after immersion in a 3.5%NaCl solution, which illustrates the aggressive attack of the corrosive medium on the mild steel surface.

In Fig. 7(a and b) shows the SEM micrograph of poly(FMA-co-GMA)/TiO_2 composite were coated before and after the corrosion. The surface of any appears smooth without the formation of significant pits, indicating the protective nature of the composite coating. On the other hand, Figure 7(c) illustrates the surface topography of the poly(FMA-co-GMA) polymer coating before and after corrosion testing. The surface exhibits roughness with numerous deep pits, which likely migrated from the substrate to the coating surface during the corrosion process through micro-pores. Upon closer inspection at higher magnification, the pits display distinct corrosion product morphology, resembling flower-like microstructures, accompanied by smaller particles that appear white in color.

The outcome of the experiment showed an improvement in the surface coverage on the mild steel, resulting in reduced contact between the steel and the corrosive medium. Thus, the presence of a protective layer with good absorbent properties effectively inhibited the corrosion of the mild steel [18]. However, the nanocomposite coating exhibited a smooth and uniform surface without any visible pits after the corrosion studies, indicating a significant enhancement in the overall corrosion resistance of the coating.

In addition, Elemental mapping of poly(FMA-co-GMA)/TiO_2 composite coating surface are shown in Figure 8. The red dots, green dots, and pink dots corresponding to the distribution states of Carbon (C), Oxygen (O), and Titania (Ti) indicated that prepared composites TiO_2 nanoparticles are successfully adsorbed on (poly(FMA-co-GMA) surface.

The EDAX- line maps provide further evidence that, the TiO_2 nanoparticles were evenly distributed across the coated surface and homogeneously dispersed within the polymer matrix, as depicted in Fig 9. [19].

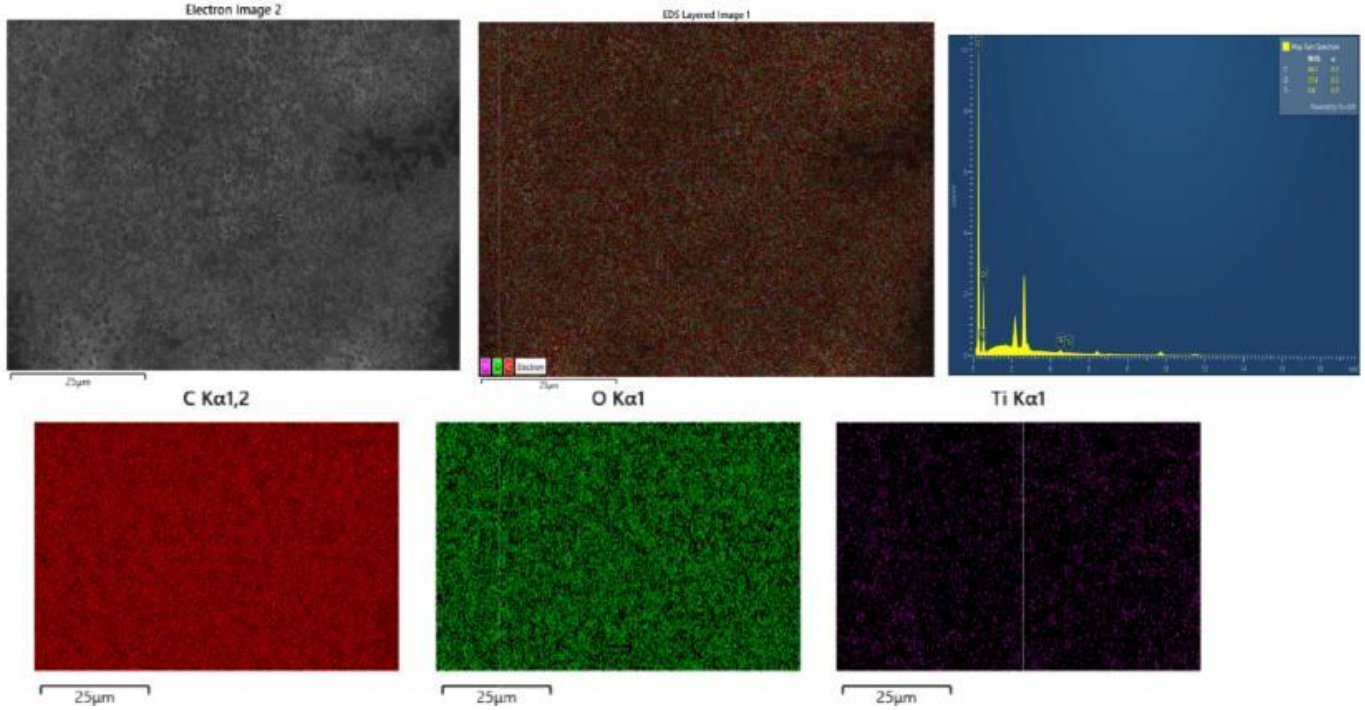

Fig. 8. poly(FMA-co-GMA)/TiO_2 composite coating on Mild steel.

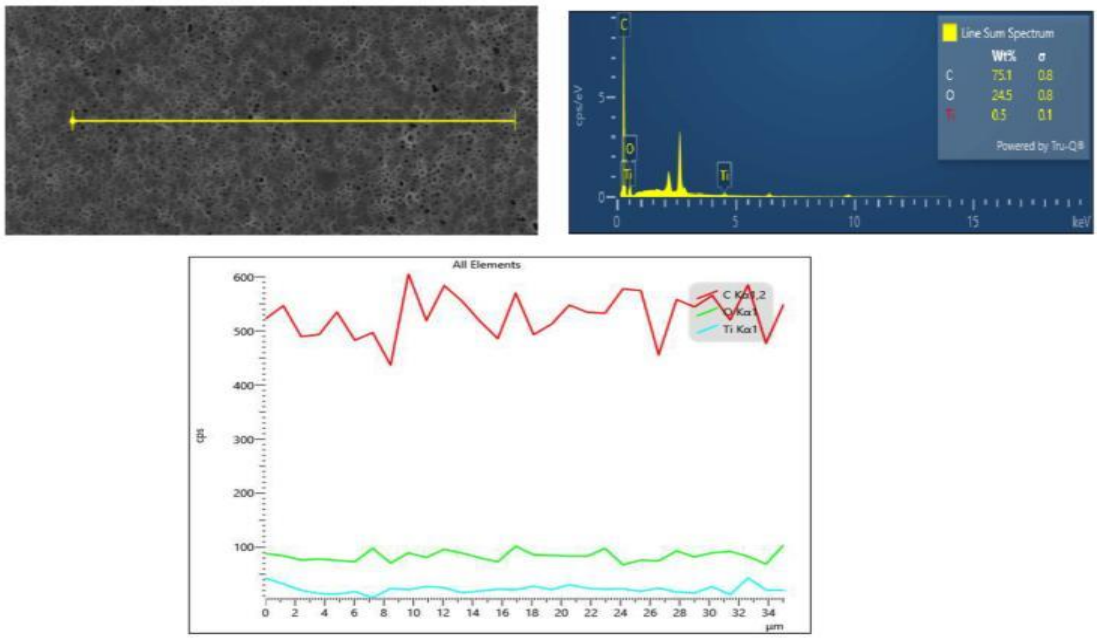

Fig. 9. EDAX-line analysis of poly(FMA-co-GMA)/TiO_2 composite coating on Mild steel.

Electrochemical Characterization:

Electrochemical Impedance Spectroscopy

The Nyquist plots of poly(FMA-co-GMA) and poly(FMA-co-GMA)/TiO_2 composite coated on mild steel specimens with different feed ratios in 3.5 wt.% NaCl solution medium is presented in Fig. 10. The EIS measurements were carried out and compared with the uncoated sample, which showed better anticorrosion efficacy. The impedance spectra of the coated specimens exhibited notable differences in both shape and size compared to the uncoated specimen. Table 2 shows the prominent existence of a substantial capacitive loop, which can be ascribed to the presence of the polymeric coating applied on the metal surface. By increasing the concentration of FMA, the capacitive loop diameter at high frequency also increases, which is related to high corrosion resistance [20]. Moreover, the sample coated with poly(FMA-co-GMA)/TiO_2 composite shows the largest loop compared with other polymer coated samples which is coincidence with inhibition efficiency (IE%).

Interestingly, increasing the concentration of FMA in the copolymer results in a larger capacitive loop diameter at high frequencies, indicating enhanced corrosion resistance. Additionally, the sample coated with poly(FMA-co-GMA)/TiO_2 composite exhibits the largest loop compared to other polymer-coated samples, coinciding with a higher inhibition efficiency (IE%).

This enhancement can be attributed to the incorporation of TiO_2 nanoparticles throughout the entire surface of the copolymer film significantly enhances the charge transfer resistance, preventing the penetration of the electrolyte [21].

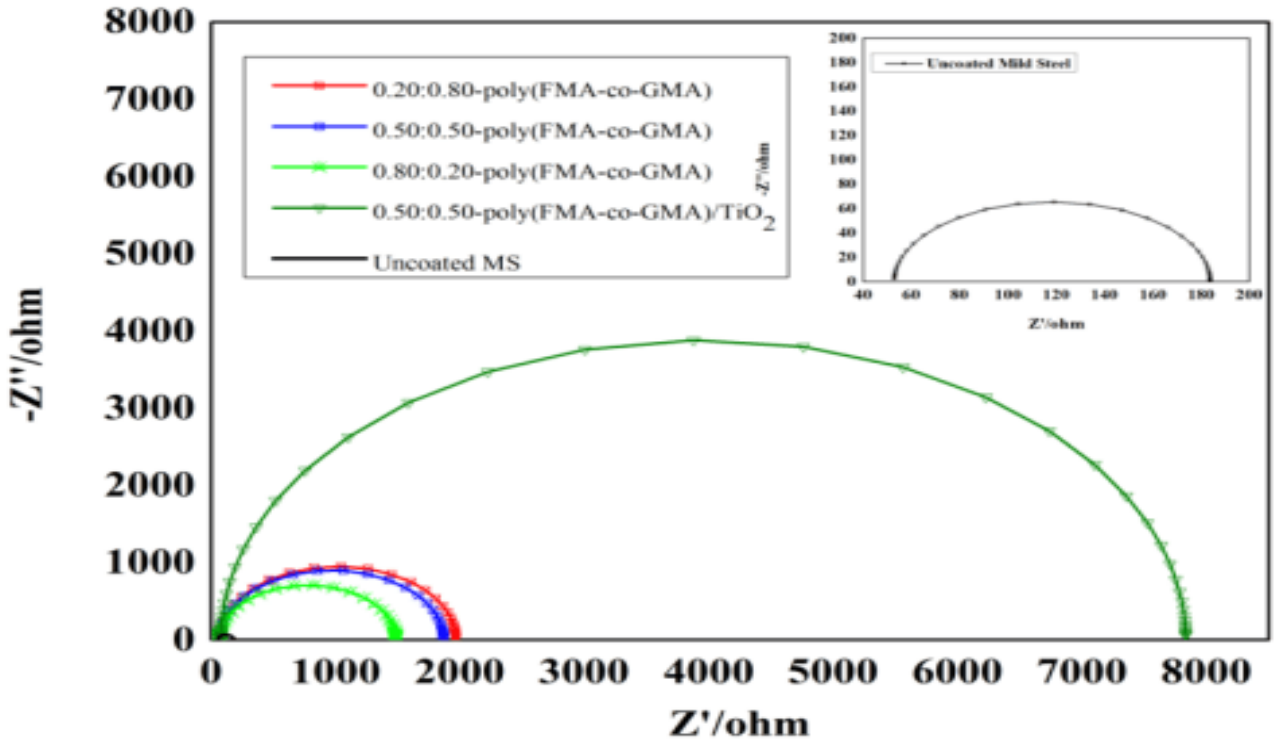

Fig. 10. Nyquist plot of poly(FMA-co-GMA) and its TiO_2 composite coating on Mild steel.

The phase angle plot of the bare substrate, shows one time constant, suggesting a severe corrosion reaction. After the substrate is coated with poly(FMA-co-GMA) coatings, one time constant appears at high-frequency region. Typically, the time constant in the high frequency region reflects the barrier performance of the coating, while that in the low frequency region is indicative of the corrosion rate. Compared with the polymer coating [22], the time constant of the TiO_2 composites coating shifts positively from 10^3Hz in the high frequency region, suggesting the improved barrier performance and lower corrosion rate.

To comprehend the experimental impedance response of each coated surface during the testing period, the impedance data was fitted to equivalent electrical circuits (Fig 11). These circuits were designed to consider either one or two time constants, allowing for a detailed analysis of the passive electrical elements involved. The proposed circuits proved to be suitable for explaining the behavior of the passive metal/electrolyte interface after prolonged immersion in a 3.5% NaCl solution [23]. The electrical components used to fit the impedance data in the equivalent circuits, are R_e, which is the electrolyte resistance, and CP and R_p, which are the constant phase element and the resistance linked with the time constant associated with the metallic surface/electrolyte electrochemical interface.

The Nyquist plots show a depressed semi-circle with the center under the real axis, whose size increases with different mole ratios of copolymer coatings, indicating a charge transfer (R_{ct}) process mainly controlling the corrosion of the mild steel. The electrochemical parameters, charge transfer resistances (R_{ct}) and double layer capacitances (C_{dl}) were calculated from the Nyquist plots [18]. The corrosion inhibition efficiency (IE%) was calculated using following equation. An increase in the concentration of polymer increases the corrosion inhibition efficiency, but the slope of the impedance curve pattern does not show any change.

S.NO	Polymer/Composite	$R_s(\Omega/cm^2)$	$R_c(\Omega/cm^2)$	$C_{dl}(F\ cm^{-1})$	Inhibition Efficiency (%)
1.	Uncoated Mild steel	50.94	130.8	7.583e-7	-
2.	0.20:0.80 – poly(FMA-co-GMA)	68.46	1418	5.24e-7	90.78
3.	0.50:0.50 – poly(FMA-co-GMA)	69.25	1801	6.33e-7	92.73
4.	0.80:0.20 – poly(FMA-co-GMA)	68.43	1902	1.13e-7	93.12
5.	0.50:0.50 – poly(FMA-co-GMA)/TiO_2	77.65	7756	1.662e-7	98.31

Table: 2. Impedance parameters of poly(FMA-co-GMA) and its TiO_2 composite coating on Mild steel in 3.5% NaCl.

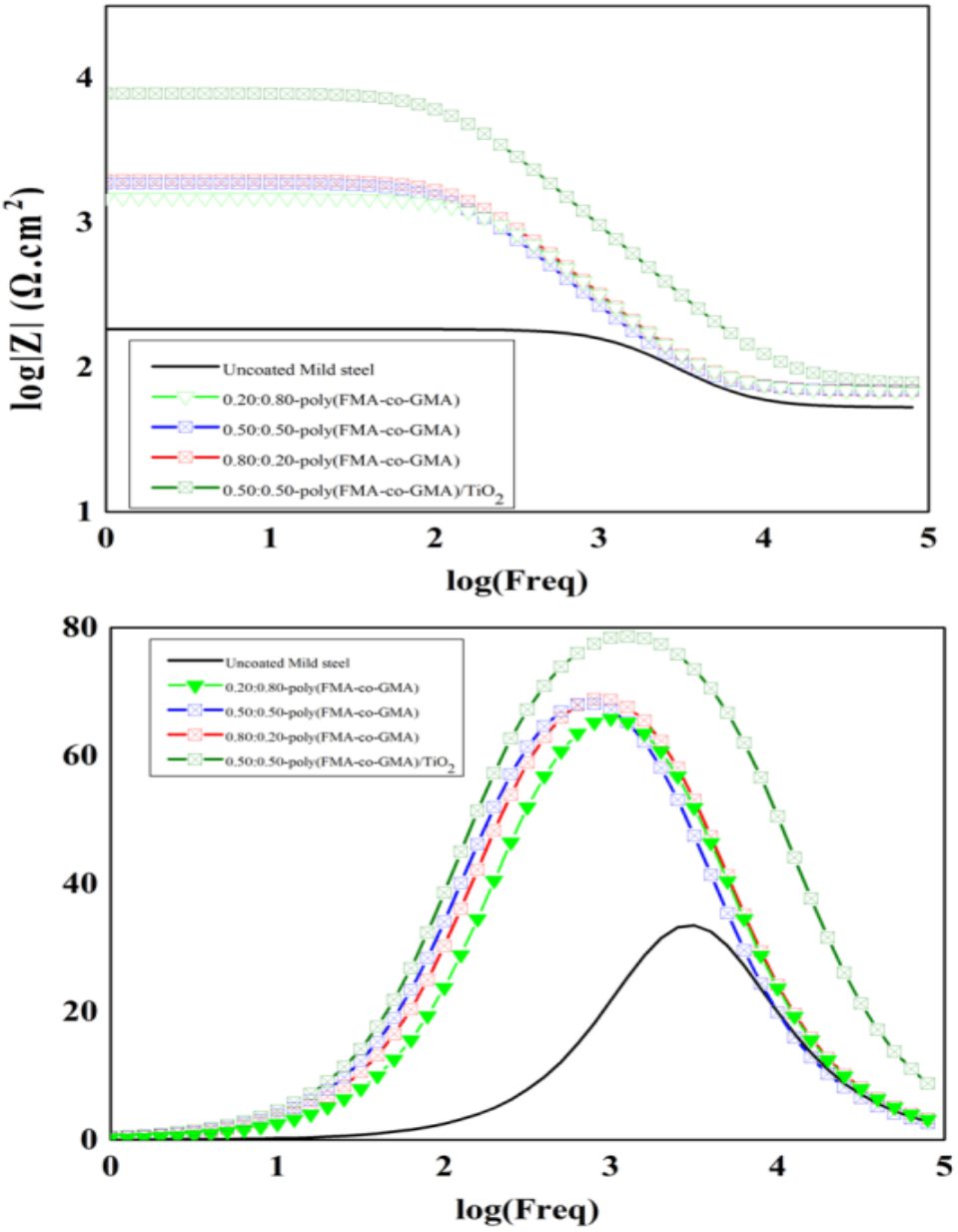

Fig. 11. Bode plot of poly(FMA-co-GMA) and its TiO_2 composite coating on Mild steel.

$$IE(\%) = \frac{(R_{ct} - R'_{ct})}{R_{ct}} X\ 100$$

Potentiodynamic Polarization studies

The potentiodynamic polarization studies were carried out for MS specimens, both for the polymer coated and uncoated of different mole ratios (0.20:0.50, 0.50:0.50 and 0.80:0.20) of poly(FMA-co-GMA) and their corresponding poly(FMA-co-GMA)/TiO_2 composites in 3.5% NaCl solution (Fig 12). The electrochemical kinetic parameters such as corrosion current density (*Icorr*), corrosion potential (*Ecorr*), Inhibition efficiency ($\eta\%$), and Corrosion (*CR*) were calculated and were given in Table 3. For the uncoated Mild steel, the *Ecorr* and *Icorr* value are 0.527 and 3.462e-5 respectively and substantially decreased by coating of polymers [24]. It shows that polymers reduce the corrosion current densities and consequently exhibits the corrosion inhibition property. The corrosion inhibition efficiency ($\eta\%$) was calculated from the corrosion current density values using the following eqn.

$$\eta(\%) = \frac{(I'_{corr} - I_{corr})}{I'_{corr}} X\ 100$$

where *I'corr* and *Icorr* are the corrosion current densities of uncoated and coated mild steel, respectively.

Corrosion current densities of poly(FMA-co-GMA)/TiO_2 composites are lower than those of the pristine polymers (0.20:0.80, 0.50:0.50 and 0.80:0.20). This clearly indicates that the TiO_2 nanoparticles embedded poly(FMA-co-GMA) adsorbs more on the metal surface, thus reducing the metal corrosion and reduce the active metal surface available for the attack of corrosive medium as well as metal dissolution.

It is due to this fact that the TiO_2 nanoparticles are arranged uniformly and cover more metal surface than the pristine polymer. It is worth mentioning that the poly(FMA-co-GMA)/TiO_2 composites showed an excellent inhibition activity of 99.96% whereas 0.20:0.80, 0.50:0.50 and 0.80:0.20 ratios of poly(FMA-co-GMA) polymeric coating showed 74.04%, 94.80% and 98.48%. As the feeding ratios of FMA are increased in polymer, the corrosion potential (Ecorr) and corrosion current density (Icorr) decreased [24]. Hence, the corrosion inhibition increases, and surface coverage also increases with FMA concentration.

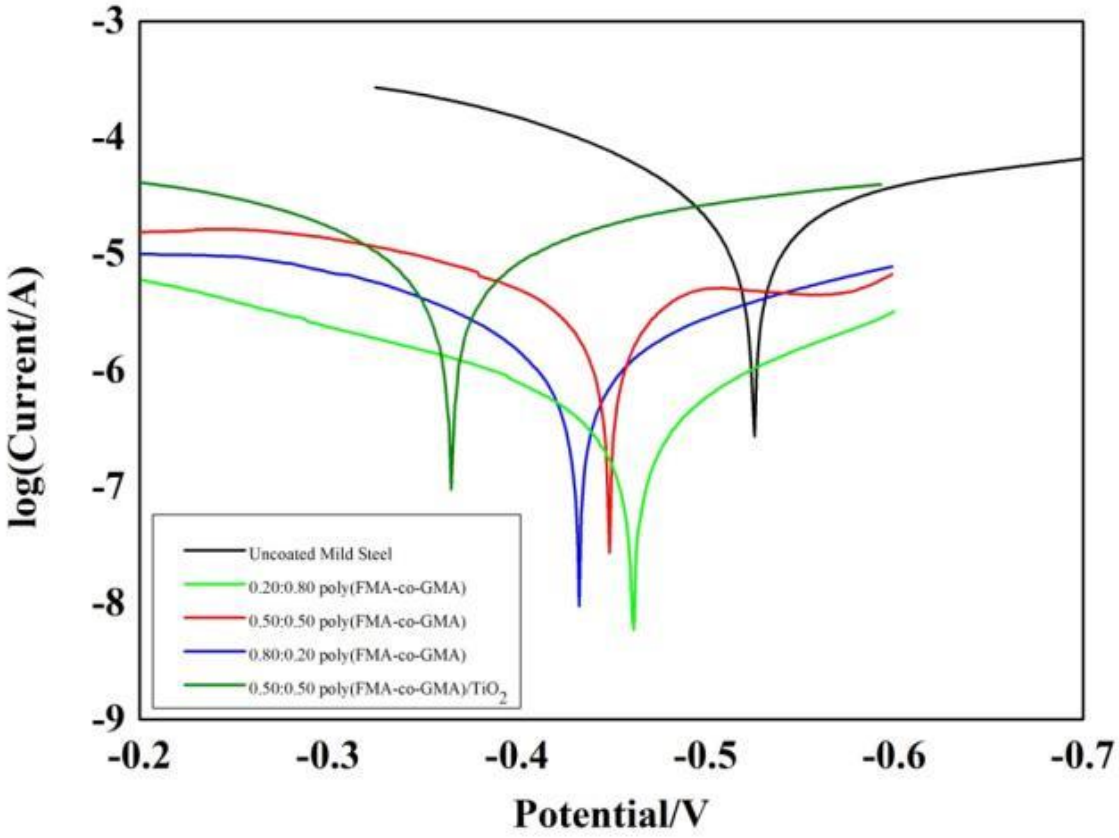

Fig. 12. Tafel plot of poly(FMA-co-GMA) and its TiO_2 composite coating on Mild steel.

Table: 3. Potentiodynamic polarizations parameters of poly(FMA-co-GMA) and its TiO_2 composite coating on Mild steel in 3.5% NaCl.

Polymer/Composite	E_{Corr} (A)	I_{Corr} (A)	Inhibition Efficiency (%)	Corrosion rate(mil/yr)
Uncoated Mild steel	0.527	3.462×10^{-5}	-	2.22×10^{3}
0.20:0.80 – poly(FMA-co-GMA)	0.462	8.986×10^{-6}	74.04	5.767×10^{2}
0.50:0.50 – poly(FMA-co-GMA)	0.449	1.800×10^{-6}	94.80	1.55×10^{2}
0.80:0.20 – poly(FMA-co-GMA)	0.433	5.273×10^{-7}	98.48	3.384×10^{1}
0.50:0.50 – poly(FMA-co-GMA)/TiO_2	0.365	1.250×10^{-5}	99.96	8.0220

CONCLUSION:

In this manuscript, we have successfully synthesized poly(FMA-co-GMA) and poly(FMA-co-GMA)/TiO_2 composites [0.20:0.80, 0.50:0.50 and 0.80:20] by free radical solution polymerization and *in-situ* polymerization techniques. Spectral and morphological studies like FT-IR, ^{1}H- and ^{13}C-Nuclear magnetic resonance spectroscopy, XRD and FE-SEM analysis. TGA studies indicated that the 0.80:0.20 ratio was more thermally stable than other copolymer compositions due to increases of Furfuryl ring in the copolymer system. The corrosion resistance performance of the Poly(FMA-co-GMA) and its TiO_2 nanocomposites coating in 3.5% NaCl solution was studied, which showed that nanocomposite has provided an effective way to fabricate a good anticorrosive coating in aggressive conditions.

The anti-corrosion study of the poly(FMA-co-GMA)/TiO_2 composite film coated on mild steel specimens were investigated and compared with poly(FMA-co-GMA) coated substrate in 3.5% NaCl solution using Tafel and electrochemical impedance spectroscopic (EIS) studies. Surface morphology studies reveals that, the nanocomposite coating exhibited a smooth and uniform surface without any visible pits after the corrosion studies, indicating a significant enhancement in the overall corrosion resistance of the coating.

Acknowledgement:

The authors are thankful to the Management of C. Abdul Hakeem College, Melvisharam, for providing the facilities to carry out this work

References:

1. Wang, Z., Huang, Y., Wang, X., Xu, Y. and Cai, F., 2022. Effects of oyster as macrofouling organism on corrosion mechanisms of a high-strength low-alloy steel. Corrosion Science, 207, p.110580.

2. Abdel-Karim, A.M. and El-Shamy, A.M., 2022. A review on green corrosion inhibitors for protection of archeological metal artifacts. Journal of Bio-and Tribo-Corrosion, 8(2), p.35.
3. Peng, T., Xiao, R., Rong, Z., Liu, H., Hu, Q., Wang, S., Li, X. and Zhang, J., 2020. Polymer Nanocomposite-based Coatings for Corrosion Protection. Chemistry–An Asian Journal, 15(23), pp.3915-3941.
4. Ashfaque, P.M., Wasi, K.A., Rehan, K.M., Banarji, J.S., Safiullah, S.M. and Basha, K.A., 2022. Anticorrosive behaviour of poly (vinyl carbazole-co-methoxy ethyl methacrylate) and its nanocomposites. Materials Today: Proceedings, 62, pp.5665-5670.
5. Nazari, M.H., Zhang, Y., Mahmoodi, A., Xu, G., Yu, J., Wu, J. and Shi, X., 2022. Nanocomposite organic coatings for corrosion protection of metals: A review of recent advances. Progress in Organic Coatings, 162, p.106573.
6. Yu, J., Yang, H., Ji, H., Zhang, X., Wang, R., Zhao, S., Wang, R. and Zhang, L., 2023. Solvent-Free Environmentally Friendly Method to Prepare Thermo-Reversible Fully Bio-Based Elastomers. ACS omega.
7. Raza, S., Zhang, J., Raza, M., Li, X., Wen, H. and Liu, C., 2021. Biomass furfural-derived green polymer microspheres: synthesis and applications for the removal of environmental pollutants from wastewater. Microporous and Mesoporous Materials, 318, p.110966.
8. Shihab, M.S., Nazari, M.H. and Fay, L., 2016. Study of inhibition effect of pyridinium salt derivative on corrosion of C1010 carbon steel in saline solution. Protection of Metals and Physical Chemistry of Surfaces, 52, pp.714-720.
9. Ashfaque, P.M., Ahmed, A.N., Safiullah, S.M., Taju, G., Majeed, S.A., Hameed, A.S. and Basha, K.A., 2022. Toxicological assessment of functional polymer with single-walled carbon nanotubes in zebrafish embryos and its gill cell line. Chemosphere, 303, p.134891.
10. Pourhashem, S., Saba, F., Duan, J., Rashidi, A., Guan, F., Nezhad, E.G. and Hou, B., 2020. Polymer/Inorganic nanocomposite coatings with superior corrosion protection performance: A review. Journal of Industrial and Engineering Chemistry, 88, pp.29-57.
11. Nasir, N.A.M., Kamaruzzaman, W.M.I.W.M., Badruddin, M.A. and Mohd Ghazali, M.S., 2023. Surface modification effects of $CaCO_3$ and TiO_2 nanoparticles in nonpolar solvents. Journal of Dispersion Science and Technology, pp.1-10.
12. Rehan, K.M., Anbarasu, B., Ashfaque, P.M., Safiullah, S.M. and Basha, K.A., 2022. Synthesis and characterization of poly (vinyl carbazole-co-ethoxy ethyl methacrylate) and its nanocomposites. Materials Today: Proceedings, 50, pp.325-330.
13. Rehan, K.M., Basha, K.A. and Safiullah, S.M., 2023. Synthesis of Poly (Glycidyl Methacrylate) Based Hybrid Materials and Evaluation of Methylene Blue Adsorption: Structural Characterization and Adsorption Behaviour. Journal of Inorganic and Organometallic Polymers and Materials, pp.1-16.
14. Nasirtabrizi, M.H., Mohebalizadeh, S. and PARCHEHBAF, J.A., 2011. Glycidyl methacrylate polymers containing indole groups: synthesis and characterization.
15. Ali, N.A., Ismail, M., Nasef, M.M. and Jalil, A.A., 2023. Enhanced hydrogen storage properties of NaAlH4 with the addition of CoTiO3 synthesised via a solid-state method. Journal of Alloys and Compounds, 934, p.167932.
16. Wang, S., Wang, N., Kai, D., Li, B., Wu, J., Yeo, J.C.C., Xu, X., Zhu, J., Loh, X.J., Hadjichristidis, N. and Li, Z., 2023. In-situ forming dynamic covalently crosslinked nanofibers with one-pot closed-loop recyclability. Nature Communications, 14(1), p.1182.
17. Zhang, D., Wang, M., Jiang, N., Liu, Y., Yu, X. and Zhang, H., 2020. Electrochemical corrosion behavior of Ni-doped ZnO thin film coated on low carbon steel substrate in 3.5% NaCl solution. International Journal of Electrochemical Science, 15(5), pp.4117-4126.
18. Thirumoolan, D., Sakthinathan, S.P. and Siva, T., 2022. Corrosion protection properties of poly ((benzoyl phenyl) methacrylate-co-methoxy ethylmethacrylate) coating on mild steel. Journal of Molecular Structure, 1264, p.133186.
19. Pawar, S.S., Naik, R.B., Billa, S., Rath, S.K., Mahato, T.K. and Kandasubramanian, B., 2023. The effect of pigment volume concentration on self-stratification and physico-mechanical properties of solvent-free silicone/epoxy coating systems. Polymer Bulletin, 80(2), pp.2045-2067.
20. Gupta, A. and Srivastava, C., 2022. Electrodeposition current density induced texture and grain boundary engineering in Sn coatings for enhanced corrosion resistance. Corrosion Science, 194, p.109945.
21. Shi, Y., Nie, Y., Xu, H., Bi, P., Chen, B., Hou, X., Ma, H. and Cao, M., 2023. Fabrication of silane-based surface coating with Ag/TiO_2 hybridization and its anti-corrosion performance on metal surface. Colloids and Surfaces A: Physicochemical and Engineering Aspects, 676, p.132241.
22. Das, C., Kastania, E., Witt, J. and Ozcan, O., 2022. Corrosion protection properties of poly (4-vinyl pyridine) containing multilayer polymeric coatings on magnesium alloy AZ31. Materials and Corrosion, 73(3), pp.427-435.
23. Xu, T., Zhao, Y., Zhou, J.H. and Hu, J.M., 2022. Composite nanocontainers synthesized by in-situ growth of metal organic frameworks on layered double hydroxides having both passive and active protecting capabilities. Progress in Organic Coatings, 164, p.106695.
24. Ouakki, M., Galai, M., Rbaa, M., Abousalem, A.S., Lakhrissi, B., Touhami, M.E. and Cherkaoui, M., 2020. Electrochemical, thermodynamic and theoretical studies of some imidazole derivatives compounds as acid corrosion inhibitors for mild steel. Journal of Molecular Liquids, 319, p.114063.